Current Applied Physics 10 (2010) 47–51

Contents lists available at ScienceDirect

Current Applied Physics

journal homepage: www.elsevier.com/locate/cap

# Fabrication and annealing effects of $SnO_2/SiO_x$ nanocables sheathed by the sputtering technique

Hyoun Woo Kim *, Seung Hyun Shim, Jong Woo Lee, Hyo Sung Kim, Mesfin Abayneh Kebede, Han Gil Na, Ju Chan Yang, Myung Ho Kong, Chongmu Lee

*Division of Materials Science and Engineering, Inha University, Incheon 402-751, Republic of Korea*

ARTICLE INFO

*Article history:*
Received 10 October 2008
Received in revised form 7 April 2009
Accepted 14 April 2009
Available online 3 May 2009

*PACS:*
81.07.-b
61.66.Fn

*Keywords:*
Nanostructures
Transmission electron microscopy

ABSTRACT

We reported an approach, in which we have produced the nano-sized crystalline tin oxide ($SnO_2$) particles with rutile structure. $SnO_2$ nanowires were coated with a shell layer of $SiO_x$ via a sputtering method. Transmission electron microscopy and elemental mapping investigations revealed that the nanostructures consisted of a crystalline $SnO_2$ core surrounded by an amorphous $SiO_x$ sheath. The annealing effects on the core-shell nanowires were investigated, revealing that the outer surface became rougher by the thermal annealing. For core-shell nanowires, a room-temperature PL measurement with a Gaussian fitting showed yellow, blue, and violet light emission bands, with the relative intensity of the yellow band showing an increase after thermal annealing. Possible PL emission mechanisms are discussed. This study reveals that the sputtering is effective for preparing the shell layers of nanocables.



## 1. Introduction

The current trend towards downsized integrated electronic and optical devices has strongly motivated the intensive study of various one-dimensional (1D) nanostructures (i.e., nanotubes, nanobelts, nanowires, and nanorods) [1,2]. In particular, one attempt has been made to create coaxial 1D structures with a core/sheath geometry, which may assist in the realization of various tailor-made functions by assembling the different features of both nanowires (as cores) and nanotubes (as sheaths) with different chemical compositions in the radial direction [3]. Indeed, the great potential has recently been demonstrated in nanodevice applications such as coaxial-gated transistors and laser diodes [4–6].

Tin dioxide ($SnO_2$) is an *n*-type semiconductor with a wide band gap ($E_g$ = 3.6 eV, at 300 K). It is well-known for its potential applications in gas sensors [7], dye-based solar cells [8], transparent conducting electrodes [9], and catalyst supports [10]. Therefore, it is natural that there has been intense interest in synthesizing $SnO_2$ 1D nanomaterials [11–13]. On the other hand, silicon (Si) and silica ($SiO_x$), which offer the possibility of integration with conventional integrated circuits (IC) technology and fabrication equipment, have attracted considerable attention due to their unique properties and promising application in mesoscopic research, nanodevices, and opto-electronics devices [14–16]. Particularly, the formation of $SiO_x$ sheaths, which exhibit excellent insulating characteristics [17] on the exterior of nanowires is essential not only to avoid interference between building blocks of a complex nanoscale circuit, but also to protect nanowires from contamination [3,18–20]. Furthermore, the $SiO_x$ coating layer is optically transparent for the visible absorption/emission of semiconductor nanowires, resulting in limited destruction of their intrinsic optical properties [21]. Thus far, Ge–$SiO_x$ [22], ZnO–$SiO_x$ [23], SiC–$SiO_x$ [24], GaP–$SiO_x$ [25], and InS–$SiO_x$ [17] core-shell nanowires have been synthesized by various processes including thermal evaporation, oxidation, carbothermal reduction and chemical vapor deposition, in which the core and shell parts of nanocables were concurrently fabricated. Additionally, $SiO_x$ sheath layers have been deposited on a pre-synthesized CdTe [26], CdS [21], Ag [27], and Au [28] core nanowires, through sol–gel or a solution-based process.

For potential application to ultra-large-scale-integration (ULSI) fabrication requiring a simple and well-controllable process, the feasibility of using two-step process was investigated, in which pre-grown $SnO_2$ 1D nanostructures are coated via a sputtering technique using a Si wafer as a target. As the ULSI fabrication technique inevitably comprises subsequent heating processes, comparisons of the samples before and after the thermal annealing were investigated in terms of their structural and photoluminescence (PL) characteristics. To the best of the authors' knowledge, this is first report on not only the synthesis of $SnO_2/SiO_x$ core-shell nanowires, but also on the wrapping of $SnO_2$ nanowires using a sputtering technique.

* Corresponding author. Tel.: +82 32 860 7544; fax: +82 32 862 5546.
*E-mail address:* hwkim@inha.ac.kr (H.W. Kim).

1567-1739/$ - see front matter © 2009 Elsevier B.V. All rights reserved.
doi:10.1016/j.cap.2009.04.009

## 2. Experimental

As an original material, $SnO_2$ nanowires synthesized by a thermal heating of Sn powders in a quartz tube are employed [29]. Subsequently, coating experiments on the as-prepared $SnO_2$ nanowires were conducted using a turbo sputter coater (Emitech K575X, Emitech Ltd., Ashford, Kent, UK). The Si sputtering target used in this experiment was a piece of polished *p*-type (1 0 0) Si wafer with resistivity of 1–30 Ω cm, which was blow-dried in $N_2$ gas. The distance between the target and the $SnO_2$ nanowires was approximately 50 mm. The sputter coater was attached to a turbomolecular pump backed by a rotary vacuum pump. The sputtering was carried out under Ar plasma at room temperature. The films were deposited for 1 min with a sputter-current of approximately 130 mA and a DC sputtering power of about 33 W. Following this, samples were subjected to thermal annealing in a quartz tube furnace at a temperature of 800 °C in $N_2$ ambient for 5 min (flow rate: 500 standard $cm^3$/min).

The structural properties of the samples were analysed by glancing angle (0.5°) X-ray diffraction (XRD) (Philips X'pert MRD diffractometer with CuKα1 radiation), field emission scanning electron microscopy (FE-SEM) (Hitachi, S-4200), and transmission electron microscopy (TEM) (Philips, CM-200) with an energy dispersive X-ray spectroscopy (EDX) installed. A TEM sample was prepared by ultrasonically dispersing the product in acetone and subsequently transferring it to a carbon-coated copper grid. PL was conducted at room temperature in a SPEC-1403 photoluminescence spectrometer with a 325 nm line from a He–Cd laser (Kimon, 1 K, Japan).

## 3. Results and discussion

The morphology and size of the resulting product were examined by observing SEM images. Fig. 1a and b show typical SEM images of the coated products before and after thermal annealing, respectively. The images indicate that both products consist of 1D structures. Moreover, Fig. 1b shows that the surface of the 1D structure became rough as a result of the thermal annealing.

An XRD was used to determine the sample phase. Fig. 2a and b show XRD patterns of the samples before and after they were coated, respectively. All recognizable diffraction peaks can be readily indexed to the tetragonal rutile structure of $SnO_2$ with lattice constants of $a = 4.738$ Å and $c = 3.187$ Å (JCPDS File No. 41-1445). By comparing Fig. 2b with Fig. 2a, it is revealed that the coating does not significantly change the XRD spectrum of the products. Therefore, the uncoated product corresponds to tetragonal $SnO_2$ with high purity, whereas the coated shell layer is amorphous and/or sufficiently thin. Fig. 2c shows an XRD pattern of the coated sample after thermal annealing. Besides the reflection peaks corresponding to the tetragonal rutile structure of $SnO_2$, a number of weak lines were found to coincide with the (2 0 0), (1 0 1), (2 2 0), and (2 1 1) peaks of the tetragonal Sn structure with lattice constants of $a = 0.583$ nm and $c = 0.318$ nm (JCPDS: 04-0673). Thus, it can be inferred that some $SnO_2$ structures were transformed, leading to the generation of Sn phases by the thermal annealing.

Fig. 3a exhibits a representative TEM image of a coated nanowire, clearly indicating that there are two segments in the structure: a rod-like core and thin coating layers (on both sides). The outer solid layer, which was formed by the second step, is relatively smooth and continuous along the nanowire. While the diameter of the core is approximately 14 nm, the thickness of the outer layer ranges from 2.6 to 4.5 nm. An enlarged TEM image as shown in Fig. 3b reveals that the core of the coated structure is single-crystalline evidenced by visible lattice fringes, whereas the shell

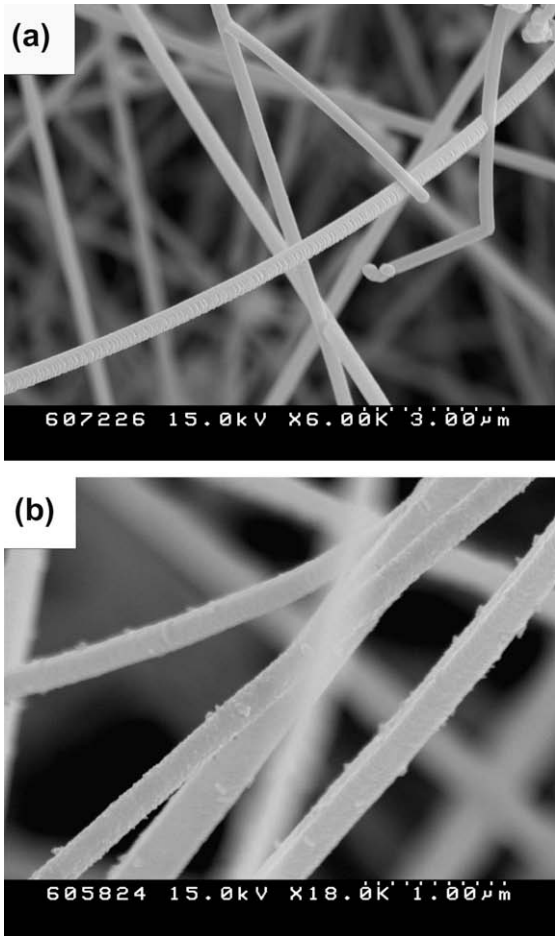


**Fig. 1.** SEM images of the coated product (a) before and (b) after thermal annealing.

is not crystalline. The inset of Fig. 3b shows the selected area electron diffraction (SAED) pattern of the coated nanowire. The SAED pattern shows a set of single-crystal electron diffraction spots corresponding to the $SnO_2$ core. In addition, the pattern shows a halo as well as a weak diffraction ring, possibly suggesting the amorphous nature of the shell layer. Fig. 3c shows an associated high-resolution TEM (HRTEM) image revealing the regular periodicity of lattice points in the core nanowire. The interplanar spacings are approximately 0.26 nm, corresponding to the (1 0 1) and $(01\bar{1})$ planes of tetragonal rutile $SnO_2$. No dislocation line can be seen in this image.

Fig. 4a shows a low-magnification TEM image of an annealed coated nanowire after thermal annealing. The nanowire shows a rough surface, which is in good agreement with the SEM observation. Fig. 4b is an enlarging TEM image of the area enclosed by the solid square in Fig. 4a. The clear contrast variation between the core and sheath suggests that the outer layer and the main body of the nanowires may consist of different materials. Fig. 4c shows a lattice-resolved HRTEM image showing an enlargement of the area enclosed by the dotted square in Fig. 4b. While the shell is not crystalline, in the core region the interplanar spacing is approximately 0.33 nm, corresponding to the $(1\bar{1}0)$ and (1 1 0) planes of tetragonal rutile $SnO_2$. Fig. 4d–f correspond to the TEM elemental mapping of the O, Si, and Sn concentrations, respectively, in the annealed core-shell nanowire. Given that the core nanowire corresponds to pure $SnO_2$, the existence of bright points in the Si elemental mapping shows that the shell layer comprises Si elements (Fig. 4e). As the diameter of the O elemental map (Fig. 4d) is apparently larger than that of the Sn elemental mapping

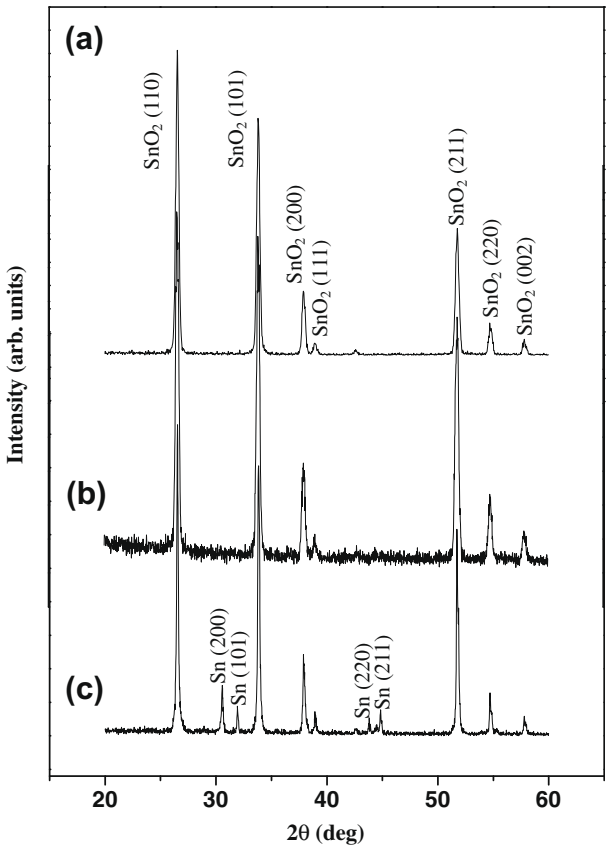


**Fig. 2.** (a) XRD pattern of uncoated product. XRD patterns of coated products (b) before and (c) after thermal annealing.

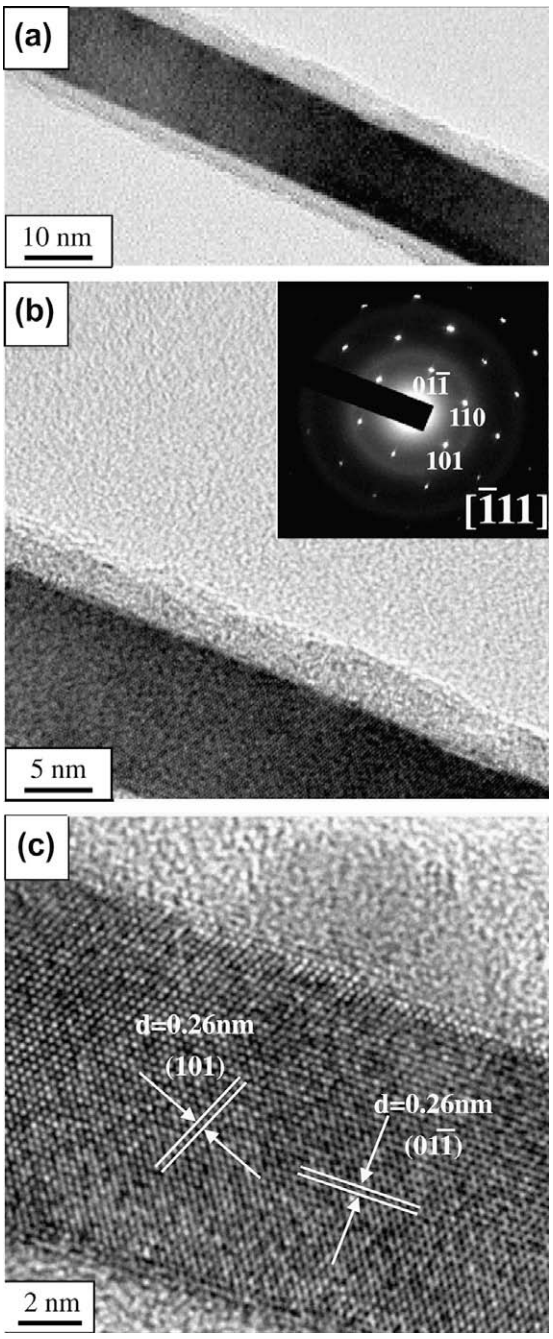


**Fig. 3.** (a) Representative TEM image of a coated nanowire. (b) Enlarged TEM image revealing that the core of the coated structure is single-crystalline, whereas the shell is not crystalline (Inset: corresponding SAED pattern). (c) HRTEM image of a coated nanowire.

(Fig. 4f), it is revealed that O is also present at the shell part of the nanowire. Since we obtained very similar elemental maps from the as-coated nanowires prior to annealing (not shown here), TEM and EDX analyses are in good agreement with what can be expected for the $SiO_x$-coated $SnO_2$ nanowires.

During the sputter deposition, the atoms or ions arrive and diffuse on the $SnO_2$ surfaces for the eventual formation of sheath layers. As shown in Fig. 3a, it can be assumed that layer growth mode has been attained, even in the room-temperature sputtering process, due to low deposition rate and crystallographically uniform (i.e., single-crystalline) $SnO_2$ surfaces. Although a nearly pure Ar atmosphere was used during the sputtering process, there is the possibility that oxygen penetrates into the growing films to generate a $SiO_x$ layer. The likely sources are $O_2$ in the Ar flow, oxygen adsorbed on the Si wafer, and residual oxygen or air leakage in the chamber. During the sputtering process, oxygen ions are formed in the plasma, replace some of the $Ar^+$ ions reaching the target, and participate in the sputtering of the target. Some oxygen atoms may be reflected from the target with high energy; others may react chemically with Si in the target and partially form a $SiO_x$ target. Another possibility is that oxygen may react directly with the Si sheath layer predeposited on the core nanowire both during and after the sputtering process. Therefore, it is expected that the sheath layers of the $SnO_2$ nanowire correspond to $SiO_x$, which is in good agreement with the experimental results.

When the thermal annealing was carried out under the same conditions on $SnO_2$ nanowires in the absence of the $SiO_x$ layers in the previous experiments, the surface was found to remain smooth. Therefore, the surface-roughening of the core-shell nanowires (as shown in Figs. 1b and 4a) is presumably due to changes in the shape of the $SiO_x$ shell layer. As the thermal annealing of $SiO_x$ produces a mixture of oxygen-rich suboxide and Si [30], in which Si clusters may be close to amorphous at the low temperature of 800 °C, it is surmised that the surface-roughening is associated with the annealing-induced phase transformation of $SiO_x$ and the subsequent coagulation of Si atoms into amorphous clusters. Further study is necessary to reveal the detailed mechanism.

Fig. 5a and b show the room-temperature PL spectra of $SiO_x$-coated $SnO_2$ nanowires without and with the subsequent thermal annealing, respectively. Fig. 5c and d show the results of a Gaussian fitting analysis for the PL spectra of the unannealed and annealed samples, respectively, indicating that the best fit of the emission was obtained with three Gaussian functions, of which the peaks

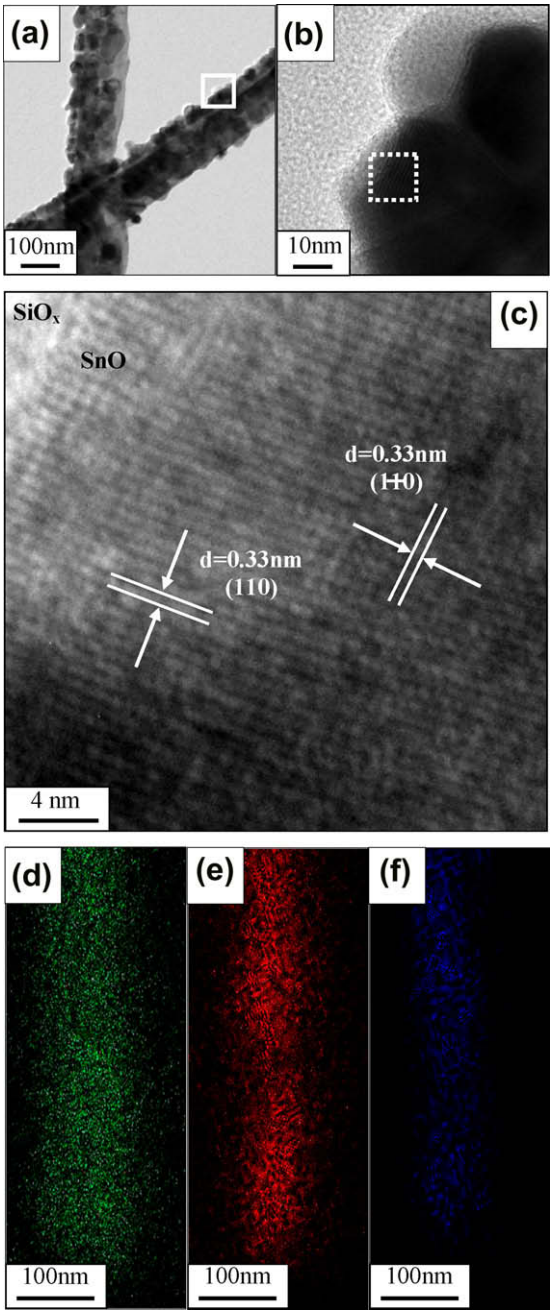


**Fig. 4.** (a) Low-magnification TEM image of a coated nanowire after thermal annealing. (b) TEM image enlarging the area enclosed by the solid square in (a). (c) Lattice-resolved TEM image enlarging the area enclosed by the dotted square in (b). TEM elemental maps of (d) O, (e) Si, and (f) Sn concentrations from a coated nanowire after thermal annealing.

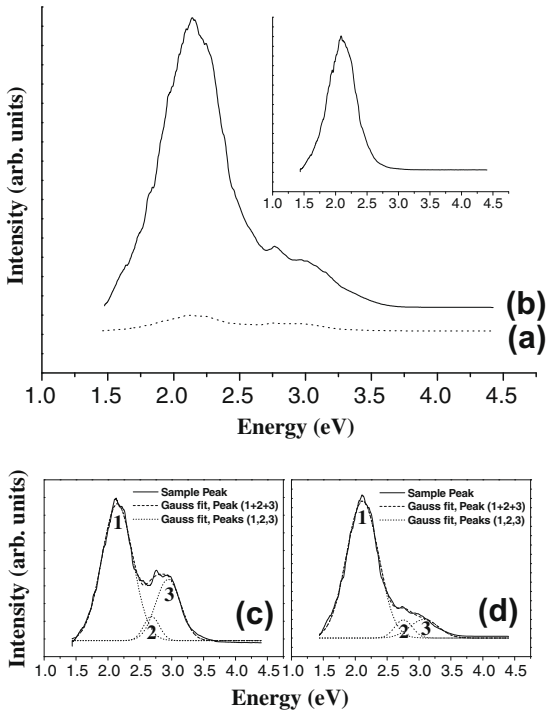


**Fig. 5.** PL spectra of coated products (a) before and (b) after thermal annealing. (Inset: PL spectrum of uncoated product.) Gaussian fitting analyses of the (c) unannealed and (d) annealed samples indicate that both emission bands are a superimposition of three major peaks.

are centered in the yellow, blue, and violet regions. While the peak position of the emission spectrum was not significantly altered, its intensity was changed by the subsequent thermal annealing. Close examination of Fig. 5a–b reveals that the PL spectra show a dominant emission peak in the region of 2.1 eV in the yellow region. In addition, two shoulder peaks exist at approximately 2.75 eV in the blue region and at approximately 3.0 eV in the violet region. In the preliminary experiments, a nearly identical yellow emission band from the uncoated $SnO_2$ nanowires was obtained, as shown in the inset of Fig. 5b. Furthermore, the yellow light emission spectrum is similar to those of the $SnO_2$ 1D nanomaterials previously synthesized using laser ablation [31] and solution-phase growth [32]. The yellow light emission of $SnO_2$ is known to be related to crystal defects or defect levels within the band gap of $SnO_2$; this is associated with O vacancies or Sn interstitials that form during the growth [31,32]. Secondly, similar to the emission band peaked at around 2.75 eV, the blue emissions with a peak position at 2.65–2.85 eV were previously observed in the PL spectrum of amorphous $SiO_x$ nanowires, an observation that is ascribed to the neutral oxygen vacancy (≡Si–Si≡) [33–36]. Thirdly, the violet emission at approximately 3.0 eV is thought to originate from the $SiO_x$ sheath layer, as similar violet emission bands at approximately 3.0–3.1 eV were observed from $SiO_x$ nanowires [33,34,36]. This violet emission is attributed to an intrinsic diamagnetic defect center, such as the twofold coordinated silicon lone pair centers (O–Si–O), which are clearly related to the high oxygen deficiency in $SiO_x$ [34,36]. The other possibility that the violet emission attributed to $SnO_2$ [37] can be excluded, as the uncoated $SnO_2$ nanowires in the present work do not exhibit the violet emission (inset of Fig. 5b).

In a comparison of Fig. 5c and Fig. 5d, it was observed that the relative intensity of the yellow emission compared to the blue and violet emissions increase with thermal annealing. With thermal annealing, it can be inferred that oxygen may diffuse from $SnO_2$ to $SiO_x$ ($x < 2$) at the core-sheath interface, generating O vacancies or Sn interstitials in the $SnO_2$ core. The appearance of Sn peaks in the annealed sample (Fig. 2c) support the assumption that O atoms tend to diffuse out from $SnO_2$ structures. Additionally, with the assumption that the blue and violet emissions in the present study are attributed to the $SiO_x$ sheath, it can be further assumed that oxygen that diffuses from $SnO_2$ enters into $SiO_x$, reducing the oxygen deficiencies in $SiO_x$, i.e., the silicon lone-pair centers (O–Si–O) and neutral oxygen vacancy (≡Si–Si≡). Although an amorphous Si cluster may exist in the annealed $SiO_x$ layers, this does not mean that clusters will emit PL. In this study, the PL properties of the core-shell nanowires were considerably enhanced by the thermal annealing, in which the relative contribution from

the core nanowire was increased as that from the sheath layer was reduced. This result will contribute to potential applications of coaxial 1D nanostructures to optoelectronic devices.

## 4. Conclusion

In summary, an approach to the synthesis of core-shell nanowires was demonstrated in this paper, in which outer layers are deposited on $SnO_2$ nanowires via sputter coating by using a Si target. The detailed morphologies, microstructures, and compositions of the resulting core-shell nanowires were characterized using SEM, XRD, TEM, and EDX. The prepared core-shell nanowires were found to possess amorphous $SiO_x$ sheaths with tetragonal rutile $SnO_2$ cores. A PL study of the core-shell nanowires revealed that the peak positions of the emission spectrum did not significantly change, whereas the relative intensity of the yellow emission was increased by the thermal annealing process. It is believed that this simple approach can be extended to prepare coaxial nanocables coated with other materials by employing different targets in a well-controllable sputtering process. This may offer opportunities for nanotechnological applications.

## Acknowledgments

This work is the outcome of a Manpower Development Program for Energy & Resources supported by the Ministry of Knowledge and Economy (MKE) (No. 37112).

## References

[1] X.F. Duan, Y. Huang, Y. Cui, J. Wang, C.M. Lieber, Nature 409 (2001) 66.
[2] M.H. Huang, S. Mao, H. Feick, H.Q. Yan, Y.Y. Wu, H. Kind, E. Weber, R. Russo, P.D. Yang, Science 292 (2001) 1897.
[3] Y. Zhang, K. Suenage, C. Colliex, S. Iijima, Science 281 (1998) 973.
[4] Y. Wu, J. Xiang, C. Yang, W. Lu, C.M. Lieber, Nature 430 (2004) 61.
[5] L.J. Lauhon, M.S. Gudiksen, D. Wang, C.M. Lieber, Nature 420 (2002) 57.
[6] H.-J. Choi, J.C. Johnson, R. He, S.-K. Lee, F. Kim, P. Pauzauskie, J. Golberger, R.J. Saykally, P. Yang, J. Phys. Chem. B 107 (2003) 8721.
[7] G. Ansari, P. Boroojerdian, S.R. Sainkar, R.N. Karekar, R.C. Alyer, S.K. Kulkarni, Thin Solid Films 295 (1997) 271.
[8] S. Ferrere, A. Zaban, B.A. Gsegg, J. Phys. Chem. B 101 (1997) 4490.
[9] Y.S. He, J.C. Campbell, R.C. Murphy, M.F. Arendt, J.C. Swinnnea, J. Mater. Res. 8 (1993) 3131.
[10] W. Dazhi, W. Shulin, C. Jun, Z. Suyuan, L. Fangqing, Phys. Rev. B 49 (1994) 282.
[11] R.-Q. Zhang, Y. Lifshitz, S.-T. Lee, Adv. Mater. 15 (2003) 635.
[12] Z.L. Wang, Z. Pan, Adv. Mater. 14 (2002) 1029.
[13] X.S. Peng, L.D. Zhang, G.W. Meng, Y.T. Tian, Y. Lin, B.Y. Geng, S.H. Sun, J. Appl. Phys. 93 (2003) 1760.
[14] S. Mann, G.A. Ozin, Nature 382 (1996) 313.
[15] A. Katz, M.E. Davis, Nature 403 (2000) 286.
[16] C.T. Kresge, M.E. Leonowicz, W.J. Roth, J.C. Vartuli, J.S. Beck, Nature 359 (1992) 710.
[17] Y.B. Li, Y. Bando, D. Golberg, Y. Uemura, Appl. Phys. Lett. 83 (2003) 3999.
[18] S. Han, C. Li, Z.Q. Liu, B. Lei, D.H. Zhang, W. Jin, X.L. Liu, T. Tang, C.W. Zhou, Nano. Lett. 4 (2004) 1241.
[19] L.J. Lauhon, M.S. Gudiksen, D.L. Wang, C.M. Lieber, Nature 420 (2002) 57.
[20] B. Min, J.S. Lee, J.W. Hwang, K.H. Keem, M.I. Kang, K. Cho, M.Y. Sung, S. Kim, M.-S. Lee, S.O. Park, J.T. Moon, J. Cryst. Growth 252 (2003) 565.
[21] A. Pan, S. Wang, R. Liu, C. Li, B. Zou, Small 1 (2005) 1058.
[22] X.-M. Meng, J.-Q. Hu, Y. Jiang, C.-S. Lee, S.-T. Lee, Appl. Phys. Lett. 83 (2003) 2241.
[23] L. Dai, X.L. Chen, X. Zhang, T. Zhou, B. Hu, Appl. Phys. A 78 (2004) 557.
[24] G.W. Meng, L.D. Zhang, C.M. Mo, S.Y. Zhang, Y. Qin, S.P. Feng, H.J. Li, J. Mater. Res. 13 (1998) 2533.
[25] S.Y. Bae, H.W. Seo, H.C. Choi, D.S. Han, J. Park, J. Phys. Chem. B 109 (2005) 8496.
[26] Y. Wang, Z. Tang, X. Liang, L.M. Liz-Marzan, N.A. Kotov, Nano. Lett. 4 (2004) 225.
[27] Y. Yin, Y. Lu, Y. Sun, Y. Xia, Nano. Lett. 2 (2002) 427.
[28] S.O. Obare, N.R. Jana, C.J. Murphy, Nano. Lett. 1 (2001) 601.
[29] H.W. Kim, N.H. Kim, J.H. Myung, S.H. Shim, Phys. Stat. Sol. (a) 202 (2005) 1758.
[30] L.X. Yi, J. Heitmann, R. Scholz, M. Zacharias, J. Phys. Condens. Matter 15 (2003) S2887.
[31] J. Hu, Y. Bando, Q. Liu, D. Golberg, Adv. Funct. Mater. 13 (2003) 493.
[32] B. Cheng, J.M. Russell, W. Shi, L. Zhang, E.T. Samulski, J. Am. Chem. Soc. 126 (2004) 5972.
[33] X.C. Wu, W.H. Song, K.Y. Wang, T. Hu, B. Zhao, Y.P. Sun, J.J. Du, Chem. Phys. Lett. 336 (2001) 53.
[34] K.H. Lee, S.W. Lee, R.R. Vanfleet, W. Sigmund, Chem. Phys. Lett. 376 (2003) 498.
[35] H. Nishikawa, T. Shiroyama, R. Nakamura, Y. Ohki, K. Nagasawa, Y. Hama, Phys. Rev. B 45 (1992) 586.
[36] D.P. Yu, Q.L. Hang, Y. Ding, H.Z. Zhang, Z.G. Bai, J.J. Wang, Y.H. Zou, W. Qian, G.C. Xiong, S.Q. Feng, Appl. Phys. Lett. 73 (1998) 3076.
[37] T.W. Kim, D.U. Lee, Y.S. Yoon, J. Appl. Phys. 88 (2000) 3759.